Research article

Identification of octyl gallate, a novel apoptosis-inducing compound for colon cancer therapy, from *Sanguisorba officinalis* L. by cell membrane chromatography and UHPLC-(Q)TOF-MS/MS

Chengyang Ni [a,1], Liang Yue [a,d,1], Mei Ran [a,b,1], Long Wang [a], Feihong Huang [a], Shuo Yang [a], Jia Lai [a], Nan Jiang [a], Xinwu Huang [a], Dalian Qin [a,c], Hua Li [a], Jie Zhou [a], Jing Zeng [a,***], Anguo Wu [a,**], Jianming Wu [b,c,*]

[a] *School of Pharmacy, Southwest Medical University, Luzhou, Sichuan, 646000, China*
[b] *School of Basic Medical Sciences, Southwest Medical University, Luzhou, 646000, China*
[c] *Education Ministry Key Laboratory of Medical Electrophysiology, Sichuan Key Medical Laboratory of New Drug Discovery and Druggability Evaluation, Luzhou Key Laboratory of Activity Screening and Druggability Evaluation for Chinese Materia Medica, Southwest Medical University, Luzhou, Sichuan, 646000, China*
[d] *Department of Pharmacy, Deyang People's Hospital, Deyang, 618000, China*

ARTICLE INFO

ABSTRACT

Colon cancer is a common gastrointestinal malignancy that ranks third in incidence among gastrointestinal cancers. Therefore, screening bioactive compounds for treatment of colon cancer is urgently needed. *Sanguisorba officinalis* L. (SO) has been demonstrated that the extractions or monomers possess potential anti-tumor effect. In this study, we firstly used cell membrane chromatography (CMC) and ultra-performance liquid chromatography coupled with (quadrupole) time-of-flight mass spectrometry (UHPLC-(Q) TOF-MS/MS) to identify a novel active ingredient, octyl gallate (OG), from SO methanol extract (SO-MtOH). HCT116 and SW620 cells lines were used for *in vitro* research, which showed OG presents great anti-colon cancer effect by inhibiting proliferation, inducing apoptosis, and repressing the migration and invasion. Furthermore, SW620 bearing athymic nude mice was used to investigate the potential antitumor activity *in vivo*, which exhibited OG treatment remarkably lessened the tumor volume. Mechanism studies showed that OG downregulated the PI3K/AKT/mTOR signaling axis and induced apoptosis by upregulating the Bax/Bcl-2 protein and the cleaved caspase-3, caspase-9. In conclusion, our research innovatively applied the method of CMC to intriguingly unearth the potential anti-colon cancer ingredient OG and demonstrated its the great antineoplastic activity, which provide a new insight for researchers efficiently developing the novel apoptosis-inducing compound for colon cancer therapy.

 * Corresponding author. School of Pharmacy, Southwest Medical University, Luzhou, Sichuan, 646000, China.
 ** Corresponding author.
 *** Corresponding author.
 E-mail addresses: zengjing@swmu.edu.cn (J. Zeng), wuanguo@swmu.edu.cn (A. Wu), jianmingwu@swmu.edu.cn (J. Wu).
 [1] These authors have contributed equally to this work and share first authorship.

1. Introduction

Currently, the frequency of colon cancer remains tall around the world and has ended up a impressive challenge for human wellbeing [1,2]. The advancement of colon cancer is influenced by various components, such as age and diet habits [3]. At present, most clinical treatments for colon cancer are based on surgical intervention supplemented with radiotherapy or chemotherapy. It does present a certain therapy, while the long-term treatment effect is suboptimal, and most chemotherapy drugs cause serious adverse reactions. Meanwhile, the prognosis of patients as well as personal satisfaction have difficulty accomplishing the ideal level. Therefore, it is of significance to seek safeguarded and convincing medicine for the treatment of colon cancer. Recently, traditional Chinese medicines (TCM) have shown unique advantages with multiple pathways and target strategies [4]. SO is a traditional Chinese medicinal herb renowned for its diverse pharmacological properties [5]. The therapeutic application of this treatment has been observed in the management of inflammatory diseases, such as airway inflammation associated with bronchial asthma [6], contact dermatitis [7], specific dermatitis [8,9], nephritis [10], and colitis for a long time [11]. In addition, SO has also been shown to have hemostatic effects, hematopoietic effects, antioxidant activity, antiviral/antibacterial effects, and treatment of leukopenia [12–14]. Even studies have been reported to present anticancer effects [15–17].

Modern pharmacological research has indicated that compounds elicit their physiological effects through direct binding to receptors located on the cellular membrane [18,19]. Thus, Cell membrane chromatography (CMC) is a biomimetic chromatographic technique that leverages the selective interaction between membrane receptors and their ligands. This method has demonstrated high efficacy in elucidating the properties of ligand-receptor interactions, as well as in screening and identifying target substances. Furthermore, CMC has shown promise in the precise quality control of pharmaceuticals [20]. For example, the epidermal growth factor receptor (EGFR) antagonists were selected and verified by using the human epidermal squamous cells (A431 cells) and human embryonic kidney cells (HEK 293 cells)-coupled CMC model [21,22], meanwhile, the potential competitive binding compound to the receptor of AGEs was investigated by human umbilical vein endothelial cell (HUVEC)-coupled CMC model [23].

Sanguisorba officinalis L., as a member of the Rosaceae family, is commonly utilized in its dried root form [24]. As a wildly used traditional Chinese medicine, it possesses an extensive history of drug useage. As early as Shennong Materia Medica, Compendium of Materia Medica and other traditional Chinese medicine works reported its efficacy, mainly reflected in cooling blood, stopping bleeding, detoxification as well as healing sores [25]. Modern research has verified that *Sanguisorba officinalis* L. possesses a wider range of pharmacological activities, including hemostasis, anti-inflammatory, anti-diarrhea, antibacterial, kidney protection, immune regulation, and anti-tumor [26–31]. Among them, the anti-tumor activity of *Sanguisorba officinalis* L. aroused great attention of researchers. Studies have investigated that radix *Sanguisorba officinalis* L. saponins have significant anti-gastric and breast cancer effects [32]. In addition, Hu Yi et al. [33] demonstrated that the tannin component of *Sanguisorba officinalis* L. tannin can effectively restrain the cell proliferation of human liver cancer cell line SMMC-7721, and Wan Chunlei et al. [34] found that the tannin component of *Sanguisorba officinalis* L. inhibit the proliferation and indece the apoptosis of HepG2 cells. However, the effect of anti-colon cancer activity of *Sanguisorba officinalis* L. has not been reported.

Octyl gallate (OG) found in *Sanguisorba officinalis* L. represents a distinctive phytochemical component, contributing to the medicinal herb's pharmacological profile. Due to its powerful antioxidant properties, OG is widely used in food, cosmetics, and pharmaceutical protectants to prevent oil oxidation and extend product shelf life. In addition to its antioxidant effects, OG has demonstrated several other potential biological activities, including antibacterial, anti-inflammatory, and anticancer effects. OG has been confirmed possessing potential anti-tumor effects such as inducing apoptosis of pancreatic cancer cells, inducing steatosis of liver cancer cells, and blocking cell cycle of breast cancer [35–37], however, its anti-colon cancer effect has not been reported yet.

In the previous study, we demonstrated that SO-MtOH can remarkably inhibit the proliferation of the human colon cancer cells SW620 *in vitro*. Hence, we hypothesized that the inhibitory effect of SW620 cells may be caused by the exact components in SO-MtOH. Thus, we applied CMC combined with (UHPLC-(Q) TOF-MS/MS method to excavate the potential active components in SO-MtOH. Ultimately, four active compounds of SO-MtOH were identified through their binding to the cellular membrane of SW620 cells using CMC. Among them, OG and ziyuglycoside II (ZYG II) can significantly reduce the viability of SW620 cells, suggesting that OG and ZYG II would be the active components in SO-MtOH for colon tumor inhibition. The identification of active constituents may contribute to the elucidation of the pharmacological and mechanistic properties of SO in the context of colon cancer, as well as to the exploration of potential novel therapeutic agents for the treatment of colon cancer.

2. Materials and methods

2.1. Reagents, Chemicals and antibodies

The chemical compounds octyl gallate, ziyuglycoside I, and ziyuglycoside II, each with a purity exceeding 99 %, were acquired from Macklin (Shanghai, China). Phosphate buffered saline (PBS) and dimethyl sulfoxide (DMSO) of hugh purity (>99.9 %) were procured from Solarbio (Beijing, China). 740 Y–P (purity = 99.63 %) was purchased from MedChemExpress (Shanghai, China).

2.2. Cell culture

L-O2 (human normal liver cell), HEK-293FT (human embryonic kidney 293FT), CCD841 CoN (human normal colonic epithelial cells), CT26 (mouse colon cancer cell CT26) and the colon cancer cell lines SW620, HCT116 and DLD-1 were provided by the China Center for Type Culture Collection (CCTCC, Wuhan, Hubei, China). L-O2, HEK-293FT, HUVEC, and HCT116 cells were cultivated in

Dulbecco's Modified Eagle Medium (DMEM, Gibco, Thermo Fisher Scientific, Waltham, MA, USA), whereas the SW620 cells were cultivated in Roswell Park Memorial Institute (RPMI 1640, Gibco, Thermo Fisher Scientific, Waltham, MA, USA). 10 % fetal bovine serum (FBS, CAT: SP10020500, Sperikon Life & Biotechnology co., ltd, Chengdu, China), penicillin-streptomycin solution (Sperikon Life & Biotechnology co., ltd, Chengdu, China) were used for cell culture, and the cells were placed at 37 °C in a humidified incubator with a 5 % CO_2. HUVECs were obtained from ScienCell (San Diego, California, USA) and cultured with Extracellular Matrix (ECM, ScienCell, San Diego, California, USA) including 5 % FBS, 1 % Endothelial Cell Growth Supplement (ECGS), penicillin-streptomycin solution at 37 °C in a 5 % CO_2 condition.

2.3. Instruments and chromatographic conditions

The UHPLC (Exion) - QTOF (×500R) MS system (AB SCIEX, USA) with a jet stream particle source was worked in negative particle mode amid the UHPLC investigation. The samples were isolated employing a Phenomenex Kinetex C18 column (100 × 2.1 mm, 100 Å) with a molecule measure of 2.6 μm (stream rate: 0.2 mL/min). The parameters of the slope elution program was connected as takes after: mobile phase A (0.1 % formic acid in water) and mobile phase B (ACN): 0–2 min, 5 % B; 2–18 min, 5–50 % B; 18–20 min, 50–100 % B; 20–25 min, 100 % B. The parameters for UHPLC-(Q) TOF-MS/MS analysis were configured as follows: a drying gas (N_2) flow rate of 120 L/min; a temperature of 250 °C; nebulizing gas, 40 psi; capillary voltage of 3500 V; fragmentor voltage of 175 V; skimmer voltage of 60 V; OCT RF V, 750 V. The collision energy (CE) was specified to −10 V, and the mass range was measured at *m/z* 100–1500 with a resolution of 15,000. After the samples were completed, the obtained data files were exported using makerview data processing software, and all the responsive charge-mass ratio and the corresponding retention time and response intensity were obtained. The blank control incubation group had no or very low response intensity, while the dose-added incubation group had a responsive and concentration-dependent charge-mass ratio, and the relevant literature was consulted based on secondary mass spectrometry information. The representative compounds were confirmed as specific binding components to SW620 cells in the methanol extract of ulmus sanguinis and as candidate compounds.

2.4. Cell membrane chromatography analysis

With high affinity and selectivity, CMC is widely utilized for screening active components from complex TCM extracts. The experiment was carried out as previously described [23,38]. In this experiment, SW620 cells coupled with the CMC model were used to identify bioactive components bound to the cell membrane. 2×10^6 cells/well of SW620 cells were cultured in 6-well plates. The cellular specimens were subjected to treatment with SO-MtOH (125, 250, 500 μg/mL). The morphology of cells in each well were observed per 0.5 h. When changes in cell morphology were observed, the medium was discarded. The cells were washed with PBS for twice. Subsequently, the cells were harvested into 2 mL EP tube with sodium citrate buffer solution (PH = 3). The cells were broken by cell ultrasonic crusher, the energy was 200 W, each ultrasound was 2 s, the interval was 5 s, and the ultrasound was 10 times. Finally, all the sample was placed in a centrifuge with the speed of 12,000 rpm for a duration of 10 min. Then, the supernatant was collected and freeze dry. After completely drying, added 200 μL methanol to each sample and mixed up by ultrasound. Cells were lysed and harvested for UHPLC-(Q)TOFMS/MS investigations. After the comparison of the components in the total ion chromatography (TIC) of SO-MtOH solution, cell lysate and final PBS wash buffer. The potential components in SO-MtOH with binding affinity were obtained.

2.5. MTT assay

The assessment of cell viability following treatment with the specified drugs was conducted using the MTT assay. In brief, cellular specimens were inoculated in 96-well microplates at a density of 3×10^3 cells per well and subsequently exposed to pharmaceutical agents for the specified duration. Following the completion of the treatment, 10 μl of MTT solution at a concentration of 5 mg/ml was introduced to each well, and the cells were subsequently incubated for an additional 4 h. Subsequently, the medium was aspirated, and 100 μl of DMSO was introduced into each well to facilitate the dissolution of the formazan. After agitating at a low velocity for 10 min at ambient temperature, the optical density at 570 nm of the solute mixture was subsequently measured using a spectrophotometer.

2.6. Transwell assays

SW620 and HCT116 cell lines were cultured in an incubator with 10 % FBS for a period of 24 h. Following this incubation, the cells were harvested and subsequently washed with PBS for twice. Subsequently, the cells were suspended in a new serum-free medium at a concentration of 5×10^5 cells/ml, and 200 μl of the cell suspension was introduced into the Boyden chamber (EMD Millipore) which had been previously coated with 50 μl of Matrigel at a final concentration of 1 mg/ml. A solution composed of 10 % FBS was introduced into the lower chamber. Following a 24 h incubation period at 37 °C, the cells within the upper chamber were subsequently removed to eliminate the noninvaded cells. The presence of invaded cells was ascertained using crystal violet staining and enumerated using light microscopy at a magnification of 200 ×. In each of three distinct experiments, a total of five fields were analyzed, with the resulting average number of migrated cells being documented.

2.7. Wound healing

The impact of OG on the migration of SW620 and HCT116 cells was assessed in accordance with established methodologies [39]. In

summary, a scratch assay was performed on SW620 and HCT116 cells using a sterile pipette tip, followed by treatment with medium containing varying concentrations of 0, 5, 10, or 20 μM OG and 40 nM paclitaxel (PTX) for a duration of 24 h. Three arbitrarily chosen perspectives along the abraded lines were captured at 0 and 24 h subsequent to OG treatment using a phase contrast inverted microscope with a 40 × magnification. The horizontal distance was measured at 0 and 24 h using Image-Pro Plus software 6.0 to quantify the migration ability of the specimen (Media Cybernetics, Inc. Rockville, MD, USA). The migration distance was determined by subtracting the distance travelled within the scratch at 24 h from the distance travelled within the scratch at 0 h.

2.8. Hoechst 33342/PT staining

The apoptosis of SW620 and HCT116 cells was identified through the utilization of Hoechst 33,342 and propidium iodide reagent staining techniques [40]. Following the treatment, the cellular specimens underwent PBS rinsing and subsequent staining with Hoechst 33,342 (10 mg/ml) and PI (10 mg/ml) for a duration of 20 min under dark conditions. Subsequently, representative cellular images containing Hoechst and PI signaling were acquired and combined. Cell apoptosis was quantified by assessing the proportion of cells exhibiting PI signals relative to those exhibiting Hoechst signals.

2.9. Flow cytometry analysis

The apoptosis rate of the cells was determined through flow cytometry analysis utilizing the Annexin V-FITC/PI apoptosis detection Kit (4A Biotech Co., Ltd., Beijing, China). In short, SW620 and HCT116 cells were cultured in 6-well plates at a seeding density of 1×10^5 cells/well. Subsequent to the treatment, cellular specimens were collected for apoptosis analysis utilizing a FACSVerse flow cytometer (BD Biosciences, San Jose, CA, USA) in accordance with the provided guidelines. FlowJo software (BD Biosciences, San Jose, CA, USA) was utilized for the acquisition and analysis of data. The data was sourced from three separate, independent experiments.

2.10. Western blotting analysis

The $1 \times$ RIPA lysis buffer consisting of protease inhibitor cocktail and phosphatase inhibitor cocktail (CST, Danvers, MA, USA) was used for the cells and tumor tissues lysis. The Quick Star Bradford $1 \times$ Dye Reagent (Bio-Rad, Hercules CA, USA) was used to determine the total protein concentration. The quality of each sample was counted and loaded with30 μg. Subsequently, each sample were loaded in SDS–PAGE for electrophoresis. Then, the polyvinylidene fluoride (PVDF) membrane was used for transferring the proteins on the SDS–PAGE to the membrane. After that, The membrane was blocked with fast blocking reagent for 20 min. Finally, the primary antibodies diluted by PBST was added to incubate the membrane for the whole night at 4 °C condition. Subsequently, all the membrane was washed with PBST for three times and incubated with secondary antibodies for 1 h at the room temperature. Finally, the hypersensitive ECL chemiluminescence detection kit (Protrintech, Wuhan, China) was used when the bands on the membrane was detected. The images of each bands was obtained by the ChemiDoc MP Imaging System (Bio-Rad, Hercules, CA, USA) and the intensities of each bands was measured by ImageJ software.

2.11. Establishment of SW620 transplanted tumor model in nude mice

Nude mice that were specific pathogen free (SPF) used in this study. The Tengxin Biotechnology Co., Ltd. (Chongqing, China) provided all the mice that we used. All the mice were kept under standard conditions, which consists of controlled temperature (22 ± 2 °C) atmosphere, humidity ($55 \% \pm 5 \%$), and a 12 h circulation of light/dark. The mice were provided unrestricted access to both commercially available standard food and purified drinking water. After a period of acclimation for seven days, the animals were subjected to random allocation into five distinct groups: the control group, 5-fluorouracil positive group (30 mg/kg), OG treatment group (15, 30, 60 mg/kg). An amount of 5×10^6 SW620 cells were subcutaneously implanted into the right flanks of mice. The commencement of treatments, with each group consisting of 6 mice, was initiated on the 12th day after the introduction of SW620 cells by injection. Weight of the body and volume of the tumor were assessed on a daily basis, with tumor volume being determined using the formula: 0.5 a × b2, where 'a' denotes the length and 'b' represents the width.

2.12. Xenograft studies

Xenotransplantation is utilized as the primary method for evaluating the effectiveness of antitumor drugs and is extensively utilized in preclinical drug screening initiatives and biomedical imaging research. The xenograft was administered in accordance with the established protocol [41]. Several of the tumor tissues underwent rapid freezing in liquid nitrogen and subsequent storage at 80 °C for subsequent protein detection. The remaining tumor tissue samples were subjected to fixation in a 4 % paraformaldehyde fixative solution (PFA) for use in hematoxylin and eosin (H&E) staining assays.

2.13. Immunohistochemistry

The tissue sections underwent a dewaxing process as the initial step. The repair solution containing citric acid was introduced and subsequently subjected to heating using a microwave oven to restore the antigen. Following the cooling process, the sections were subjected to a 15 min incubation in a 3 % H_2O_2 solution to suppress endogenous peroxidase activity. Subsequently, they were washed
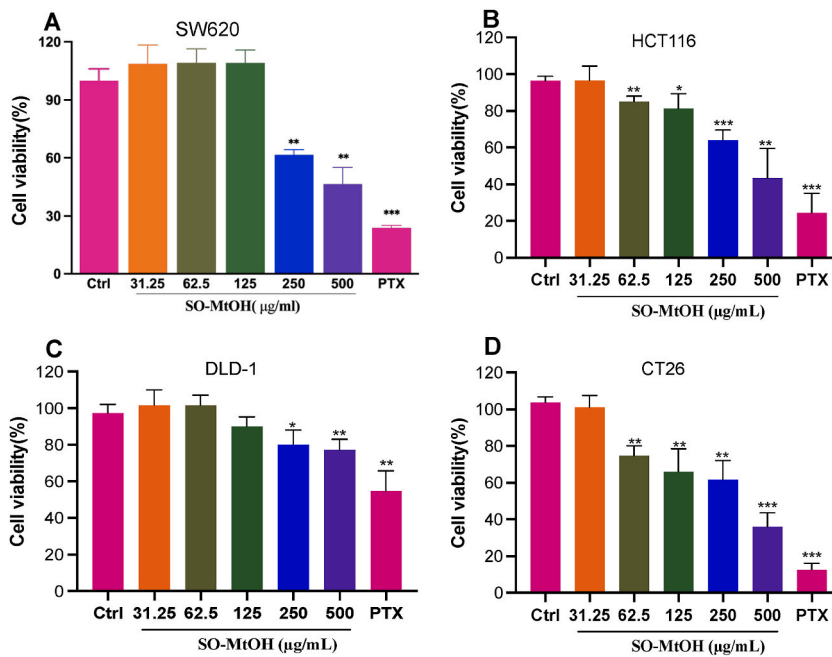
Fig. 1. The inhibitory impact of SO-MtOH on cell proliferation in SW620 cells. **(A)** The cellular viability of SW620 cells following a 48 h treatment with SO-MtOH was evaluated utilizing the MTT assay. **(B)** The viability of HCT116 cells following a 48 h treatment with SO-MtOH was assessed using the MTT assay to determine cell viability. **(C)** The cellular viability of SO-MtOH in DLD-1 cells following a 48 h treatment was quantified using the MTT assay. **(D)** The viability of CT26 cells following a 48 h treatment with SO-MtOH was assessed using the MTT assay to determine its impact on cell viability. The data reported in this study represents the mean ± standard deviation (SD) of six independent experiments. The data was analyzed using one-way analysis of variance (ANOVA) with Dunnett's 154 and two-way ANOVA with Tukey's 862 multiple comparisons test. The significance levels for the comparisons are denoted as follows: *$P < 0.05$, **$P < 0.01$, and ***$P < 0.001$ vs. control.

thrice with PBS and then incubated in a blocking buffer consisting of 0.3 % Triton-X-100 and 5 % serum in PBS for a duration of 1 h. The sections were subjected to incubation with 50 μl of caspase-3 (1:200), caspase-9 (1:100), Bax (1:400), and Bcl-2 (1:100) primary antibodies overnight at 4 °C. Following this, the sections were exposed to an HRP-labeled secondary antibody and subsequently reacted with 3,3′-diaminobenzidine (DAB) as a substrate. They were then counterstained with hematoxylin for a duration of 1 min and subsequently rinsed with distilled water. Subsequently, the slices underwent dehydration and were subsequently treated with neutral gum for fixation. The investigation involved microscopic imaging of cells displaying a positive signal, which was accomplished using the Image-Pro Plus 6.0 [42].

2.14. H&E staining assay

As per the guidelines provided by the manufacturer, the paraffin sections underwent a process of dewaxing, consisting of two washes with xylene, followed by rehydration using a gradient series of ethanol concentrations and double distilled water. Subsequently, the slides underwent staining with Harris hematoxylin (H&E) solution for a duration of 8 min, followed by a 5 min washing in running tap water. Following the washing procedure, the slides underwent differentiation in a 1 % acid alcohol solution for a duration of 30 s, followed by rinsing in running tap water for a period of 1 min. Subsequently, the slides underwent counterstaining in an eosinphloxine solution for a duration of 30 s, followed by dehydration in 95 % and 100 % alcohol for a period of 1 min. Ultimately, the slides were affixed with neutral gum and subsequently, illustrative visual data was obtained through the employment of a fluorescence microscope (Nikon ECLIPSE 80i, Tokyo, JPN).

2.15. Data analysis

Statistical analyses were performed in order to determine differences between groups, utilizing Student's *t*-test or one-way analysis of variance (ANOVA) in Prism 5.01 software. Statistical significance was determined for differences with a p-value less than 0.05 (ns *P* > 0.05, *$P < 0.05$, **$P < 0.01$, ***$P < 0.001$).
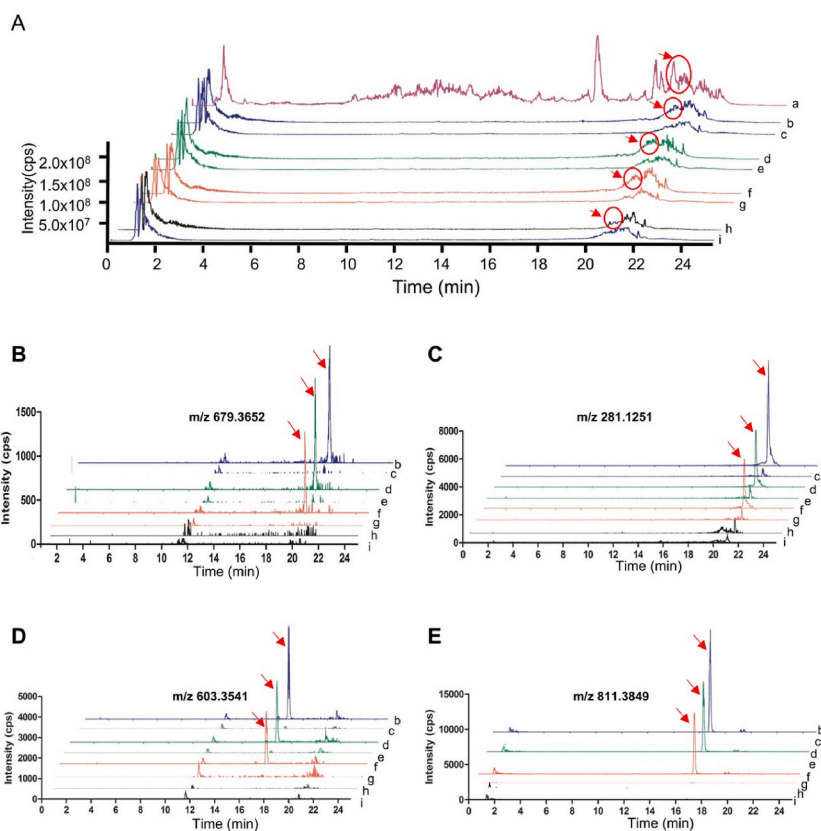
Fig. 2. The TICs of the CMC samples collected and screened of the mass-to-charge ratio (m/z) from SO-MtOH treatments. SW620 cells were incubated with SO-MtOH (0, 125, 250, 500 μg/ml) for 4 h. Following the incubation period, chemical constituents lacking binding affinity to the cellular membrane were removed through a wash with PBS, whereas constituents demonstrating binding capabilities with the cellular membrane were preserved for subsequent analysis. The cells were subsequently disrupted using an ultrasonic method in a PBS solution. The lysate solution underwent centrifugation, subsequent drying, and subsequent reconstitution in methanol. (**A**) The TICs of total SO-MtOH were recorded by UHPLC-(Q) TOF-MS/MS. (**B, C, D, E**) Response intensity of mass spectrometry in cell lysate (m/z 679.3652; m/z 281.1251; m/z 603.3541; m/z 811.3849). a: 500 μg/mL SO-MtOH; b,d,f,h: SW620 cell lysate solution with SO-MtOH (0, 125, 250, 500 μg/mL) treatments; c,e,g,i: the final PBS wash solution (0, 125, 250, 500 μg/mL).

Table 1
The identification of the specific binding compounds of SO-MtOH was achieved through the utilization of CMC analysis.

Peak No	m/z	RT (t_R/ min)	Intensity of ionic response in SO-MtOH treatment (μg/mL)					Relative absorption ratio (%)	Chemical	MS²
			0	125	250	500	standard solution			
1	679.3652	19.99	33.37	496.10	602.91	786.86	564631.37	0.14	ziyuglycoside III	633,471 [43]
2	603.3541	16.86	35.51	1467.25	1481.41	1896.05	385660.03	0.49	ziyuglycoside II	585 [44]
3	281.1251	21.11	888.90	15991.40	18944.4	32858.81	222970.50	14.74	Octyl gallate	169 [45]
4	811.3849	19.28	3.06	163.45	192.28	314.66	18304.96	1.72	ziyuglycoside I	603

Note: Relative adsorption rate (%) = intensity incubation (500 μg/ml)/intensity standards solution of SO-MtOH (500 μM).

3. Results

3.1. Identification of components with anti-proliferative effect from SO-MtOH by CMC

Initially, the anti-proliferative impact of SO-MtOH was validated through the implementation of the MTT assay. The results exhibited that 250 and 500 μg/ml SO-MtOH significantly inhibited the viability of SW620, HCT116, DLD-1 and CT26 cells after 48 h of treatment (Fig. 1 A, B, C, D). Then, CMC was employed to identify the potential components in SO-MtOH that have anti-proliferative effect in SW620 cells. The TIC showed that the components (with retention times (RT) of approximately 20 – 22 min) in the lysates of
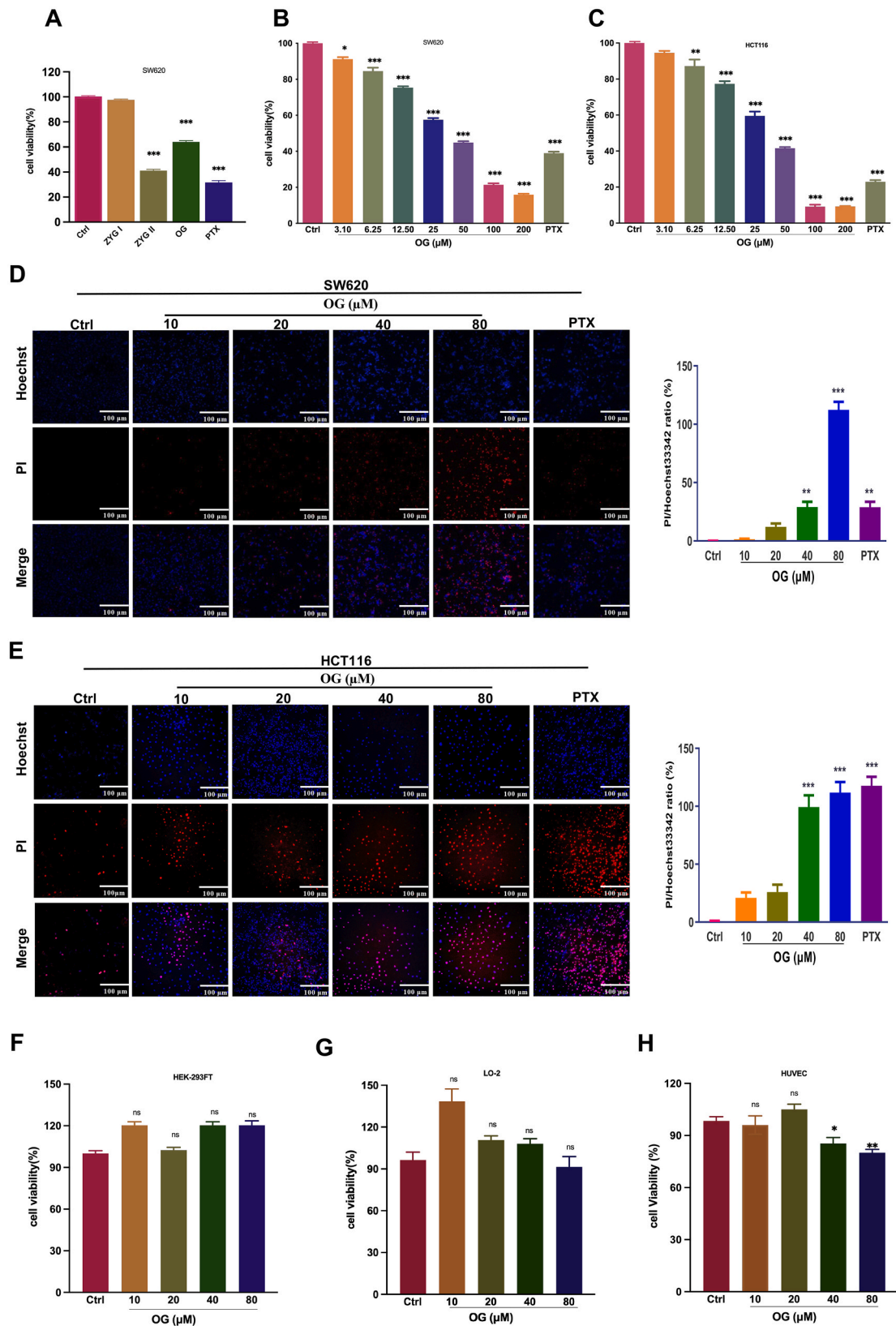
Fig. 3. Anti-proliferation effect of OG. (**A**) The cell viability of BAF (ZYG I, ZYG II, OG) in SW620 cells for 72 h treatment (mean ± S.D., n = 4); PTX as a positive control. (**B, C**) The cellular viability of SW620 and HCT116 after the 48 h treatment of OG, respectively (mean ± S.D., n = 4). (**D, E**) Cells were subjected to incubation with a combination of Hochest 33,342 and PI to capture cells with fluorescent signal under a fluorescence microscope. A bar chart depicting the comparative density of PI to hochest33342. (**F, G, H**) The impact of OG on cell viability of L-O2, HEK293FT and HUVEC cells (mean ± S.D., n = 4). The data reported in this study represents the mean ± standard deviation (SD) of four independent experiments. The data was analyzed using one-way analysis of variance (ANOVA) with Dunnett's 154 and two-way ANOVA with Tukey's 862 multiple comparisons test. The significance levels for the comparisons are denoted as follows: $*P < 0.05$, $**P < 0.01$, and $***P < 0.001$ vs. control.
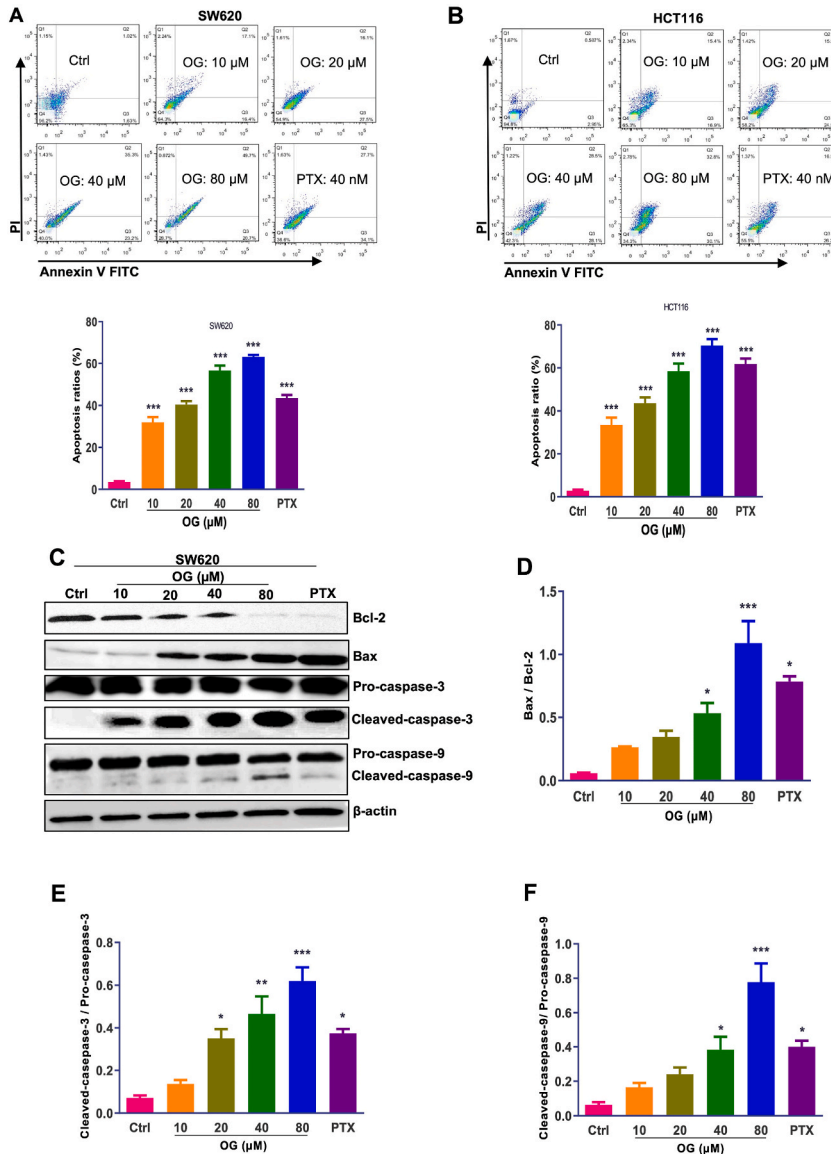
Fig. 4. OG induces apoptosis in SW620 and HCT116 cells. The SW620 and HCT116 cell lines were subjected to treatment with varying concentrations of OG (0, 10, 20, 40, 80 μM) and a fixed concentration of PTX (40 nM) for a duration of 48 h. (**A, B**) The cells were treated with trypsin and subsequently cultured with a combination of Annexin V - FITC and PI, followed by flow cytometric analysis. A graphical representation in the form of a bar chart illustrating the rate of apoptosis in a biological system. (**C, D, E, F**) The cellular protein was subsequently extracted to investigate the presence of caspase-3, caspase-9, Bax, Bcl-2, and β-actin using western blotting analysis. The bar chart depicts the comparative densities of cleaved-caspase-3 to pro-caspase-3, cleaved-caspase-9 to pro-caspase-9, and Bax to Bcl-2. The data reported in this study represents the mean ± standard deviation (SD) of three independent experiments. The data was analyzed using one-way analysis of variance (ANOVA) with Dunnett's 154 and two-way ANOVA with Tukey's 862 multiple comparisons test. The significance levels for the comparisons are denoted as follows: $*P < 0.05$, $**P < 0.01$, and $***P < 0.001$ vs. control.

A

B

C

D
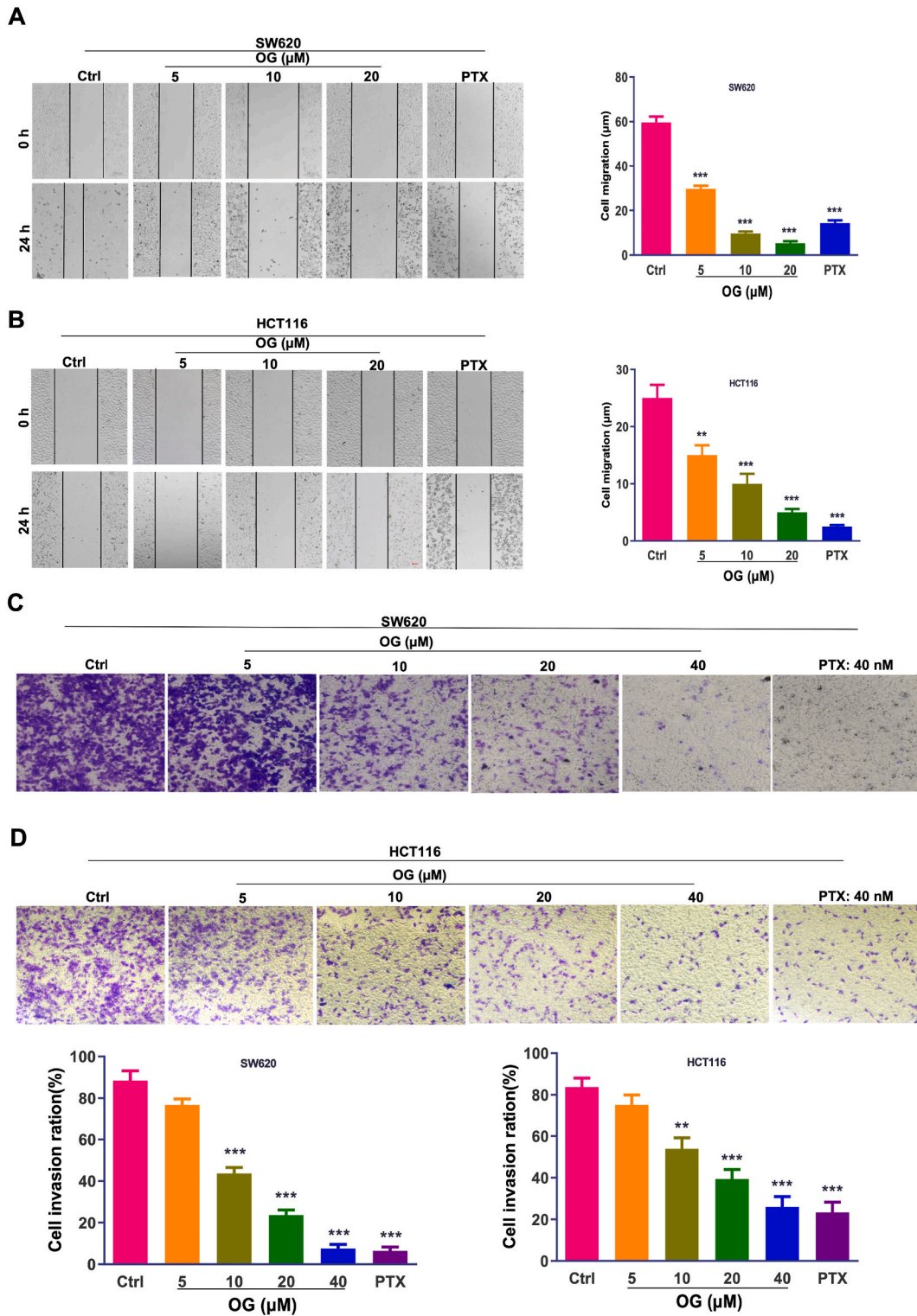
Fig. 5. OG demonstrates a capacity to suppress the migration and invasion of SW620 and HCT116 cells. SW620 and HCT116 cells were treated with OG (0, 10, 20, 40 μM) and PTX (40 nM) for 24 h. (**A, B**) The wound-healing analysis demonstrated the migratory capacity of SW620 and HCT116 cells. A bar chart illustrating the migratory distance of SW620 and HCT116 cells. (**C, D**) Transwell assay was utilized to assess the invasive properties of SW620 and HCT116 cells. The bar chart depicted illustrates the invasion activity of SW620 and HCT116 cells. The data reported in this study represents the mean ± standard deviation (SD) of three independent experiments. The data was analyzed using one-way analysis of variance (ANOVA) with Dunnett's 154 and two-way ANOVA with Tukey's 862 multiple comparisons test. The significance levels for the comparisons are denoted as follows: $*P < 0.05$, $**P < 0.01$, and $***P < 0.001$ vs. control.

cells incubated with SO-MtOH (0, 125, 250, 500 μg/mL) were increased in a concentration-dependent manner. Besides, these components could be found in SO-MtOH without in the final PBS wash buffer (Fig. 2A). Further analysis found that the mass-to-charge ratios (m/z) of the 4 potential components were 679.3652, 281.1251, 603.3541, and 811.3849 (Fig. 2B, C, D, E). By comparing the data in the literature and the chromatograms of standards (Supplemental Figs. 1A, B, C, D), these chemical compounds were confirmed to be ziyuglycoside I (ZYG I), ziyuglycoside II (ZYG II), ziyuglycoside III (ZYG III) and OG (Table 1).

3.2. OG inhibits the cells viability of SW620 and HCT116

To approve the screening result, we firstly analyzed the viability of SW620 cells treated with ZYG I, ZYG II and OG by MTT measure. The results exhibited that 20 μM ZYG II and OG essentially restrained the practicality of SW620 cells after 72 h of treatment (Fig. 3A). ZYG II has been documented to elicit apoptotic effects on colon cancer cells by means of both caspase-dependent and caspase-independent pathways. These effects entail downregulation of Bcl-2 expression, mitochondrial targeting, modulation of ROS production, and translocation of apoptosis-inducing factor to the nuclei [46]. This provides evidence that CMC is convincing. Consequently, the subsequent experiment was centered on investigating the potential antitumor properties and mechanism of action of OG both in *in vitro* and *in vivo* settings. The results of the MTT assay indicated that OG exhibited a dose-dependent decrease in cell viability and a concurrent inhibition of growth in SW620 and HCT116 cells (Fig. 3B and C, Supplemental Figs. 2A and B). The IC$_{50}$ values were calculated as 35.2 and 32.2 μM, respectively (Supplemental Figs. 2C and D). Additionally, OG demonstrated considerable cytotoxic effects on DLD-1 and CT26 cells in comparison to the control group (Supplemental Figs. 3A and B). In addition, the Hoechst/PI-stained cell images showed that the OG at varying doses and time intervals (24 and 48 h) resulted in a dose- and time-dependent increase in the proportion of cells exhibiting PI signals relative to Hoechst signals. These findings indicate that OG may potentiate cell death in SW620 and HCT116 cells (Fig. 3D and E, Supplemental Figs. 3C and D). and cell cycle analysis showed DNA cytometry in G1 phase increased after treatment of OG 10–80 μM (Supplemental Figs. 4F and G). Moreover, we also measured the cytotoxicity of OG at concentrations of 10–80 μM in normal cell lines, including LO2, HEK293FT and HUVECs, the results showed no cytotoxicity (Fig. 3F, G, H). What is more, the results of apoptosis analysis showed LO2, HEK293FT cells treated with OG 10–80 μM showed no significant apoptosis ratio in comparison to the control (Supplemental Figs. 4A, B, C, D) and the cytotoxicity of OG on the CCD841 CoN cells was measured, which showed OG at concentrations of 10–80 μM possessed no significant cytotoxicity in comparison to the control (Supplemental Fig. 3E). Collectively, the use of OG without cytotoxicity on normal cells demonstrated a significant inhibition in the proliferation of SW620 and HCT116 cells.

3.3. OG induces apoptosis in SW620 and HCT116 cells

To investigate the mechanism of cellular death in SW620 and HCT116 cells, the apoptosis rate was assessed using flow cytometry and an Annexin V-FITC/PI apoptosis detection kit. The results depicted in Fig. 4A and B illustrate that OG substantially elevated the rate of apoptosis in SW620 and HCT116 cells in a manner that was proportional to the dosage administered. Furthermore, the quantification of apoptosis-related proteins was conducted through Western blot analysis. The findings indicated that the administration of OG led to a progressive elevation in the protein levels of cleaved caspase-3 and caspase-9, as well as the ratio of Bax to Bcl-2 in a dose-dependent manner (Fig. 4C, D, E, F). Therefore, OG induces apoptosis in SW620 cells.

3.4. OG inhibits the migration and invasion of SW620 and HCT116 cells

The process of cancer cell metastasis holds significant importance in the progression of tumors, as it encompasses the infiltration and breakdown of the adjacent extracellular matrix and tissues. Subsequently, an enhanced examination was conducted to assess the suppressive impact of OG on the migratory and invasive capacities of SW620 and HCT116 cells using the wound-healing assay and Transwell filters coated with Matrigel. The findings indicated that OG greatly suppressed the migration of SW620 and HCT116 cells in a manner that was proportionate to the dosage administered, as depicted in Fig. 5A and B. Furthermore, it is noteworthy that Fig. 5C and D depict the inhibitory effect of OG in a dose-dependent manner on the invasion of SW620 and HCT116 cells. Hence, it can be inferred that OG exerts an inhibitory effect on the migratory and invasive capabilities of SW620 and HCT116 cells.

3.5. OG inhibits the PI3K/AKT/mTOR signaling pathway

Recent research findings indicate that the PI3K/AKT/mTOR signaling pathway plays a pivotal role in enhancing cell proliferation and promoting cell survival [47]. In order to investigate the molecular mechanisms through which OG inhibits colon cancer, our study sought to assess the impact of OG on the protein expression of PI3K, AKT, and mTOR in SW620 cells using western blotting analysis. As
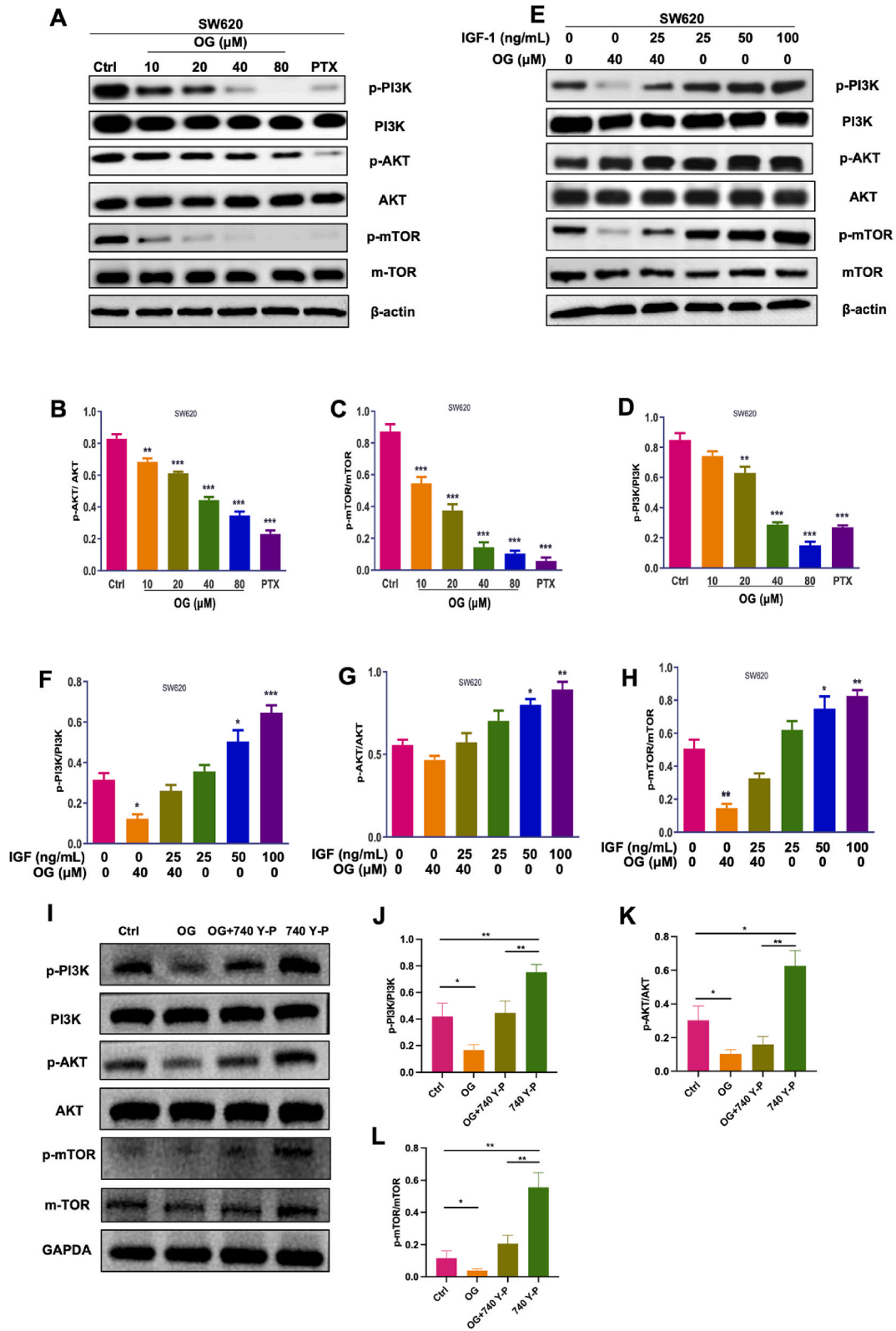
Fig. 6. Initiates programmed cell death through the PI3K/AKT/mTOR signaling pathway. The SW620 cell line was subjected to treatment with varying concentrations of OG (0, 10, 20, 40, 80 μM) in addition to PTX (40 nM) over a 48 h. The cellular protein was subsequently isolated and used for the detection of PI3K, p-PI3K, AKT, p-AKT, mTOR, p-mTOR, and β-actin through Western blot analysis. (**A**) The bands of PI3K, p-PI3K, AKT, p-AKT, mTOR, p-mTOR and β-actin of SW620 cells. (**B, C, D**) Summary bar graph of p-PI3K to PI3K, p-AKT to AKT, p-mTOR to mTOR of SW620 and HCT11. (**E**) The SW620 cells underwent a co-treatment with OG and IGF-1 for a duration of 48 h. The cellular protein was subsequently isolated in order to carry out detection of PI3K, p-PI3K, AKT, p-AKT, mTOR, p-mTOR, and β-actin using Western blot analysis. (**F, G, H**) Summary bar graph of p-PI3K to PI3K, *p*-AKT to AKT, p-mTOR to mTOR. (**I**) SW620 cells were subjected to a co-treatment of OG (80 μM) and 740 Y–P (25 μM) for a duration of 48 h. The cellular protein was subsequently collected and analyzed via Western blot for the detection of PI3K, p-PI3K, AKT, p-AKT, mTOR, p-mTOR, and GAPDH. (**J, K, L**) Summary bar graph of p-PI3K to PI3K, p-AKT to AKT, p-mTOR to mTOR. The data reported in this study represents the mean ± standard deviation (SD) of three independent experiments. The data was analyzed using one-way analysis of variance (ANOVA) with Dunnett's 154 and two-way ANOVA with Tukey's 862 multiple comparisons test. The significance levels for the comparisons are denoted as follows: $*P < 0.05$, $**P < 0.01$, and $***P < 0.001$ vs. control.

shown in Fig. 6 A, B, C, D, OG significantly inhibited the phosphorylation of PI3K, AKT, and mTOR in SW620 cells. On the other hand, the PI3K/AKT pathway activator IGF-1 dose-dependently increased the expression of p-PI3K, p-AKT and p-mTOR in SW620 cells and reversed the inhibitory effect of OG on the expression levels of p-PI3K, p-AKT and p-mTOR (Fig. 6 E, F, G, H). Meanwhile, another PI3K/AKT pathway activator 740 Y–P was utilized to further investigated the regulation effects of OG, the findings indicate that the treatment of SW620 cells with 740 Y–P led to a significant upregulation of p-PI3K, p-AKT, and p-mTOR., while treated with 740 Y–P and OG, the upregulation was interrupted (Fig. 6 I, J, K, L). Collectively, the findings indicate that OG suppresses the growth of SW620 colon cancer cells by obstructing the PI3K/AKT/mTOR signaling pathway.

3.6. OG inhibits tumor growth in SW620 bearing athymic nude mice

In order to further elucidate the potential therapeutic impact of OG in colon cancer, subcutaneous injection of SW620 cells into nude mice was conducted to verify the inhibitory effect of OG on tumor growth and characterize its underlying mechanism. Body weight and tumor weight were measured bi-daily. Following pharmaceutical intervention, it was observed that the tumor volume in the OG and 5-FU cohorts exhibited a noteworthy decrease in comparison to the vehicle group (Fig. 7A and B). Concurrently, there was a substantial reduction in tumor weight observed in the OG and 5-FU groups, while no significant alterations in body weight were noted (Fig. 7C, Supplemental Fig. 5A). Subsequently, the neoplastic tissues underwent Hematoxylin and Eosin (H&E) staining, as well as detection of protein expression via Immunohistochemistry (IHC) and Western blotting. The H&E staining analysis demonstrated that both OG and 5-FU exerted a significant inhibitory effect on the proliferation of SW620 cells (Fig. 7D). What is more, The H&E staining of liver and kidney exhibited no significant changes in cell morphology after treatment of OG, which indicated the dosages of OG was relative safe (Supplemental Figs. 5B and C). Furthermore, there was a marked increase in the expression of proteins linked to the process of apoptosis, such as caspase-3, caspase-9, and Bax, in addition to a decreased expression of Bcl-2, a protein with anti-apoptotic properties, in the OG and 5-FU groups. (Fig. 7E, F, G, H, I). Taken together, OG exhibits potent anti-colon cancer activity *in vivo*.

4. Discussion

TCMs have compelling anticancer effects, such as Taxol isolated from *Taxus chinensis (Pilg.) Rehd*, which has been widely used in the clinic for antitumor chemotherapy [34]. Apart from that, some clinically essential anticancer drugs, such as colchicin, vinblastine and vincristine, are isolated from TCMs. Chinese medicine monomers have become one of the critical sources for antitumor drug screening. However, the identification of effective ingredients from TCMs has been proven to be thorny and inefficient. Partly, the reasons could be concluded to be that the composition of TCMs is complex and unstable. With the concept of target screening, molecular fishing, click chemistry and CMC coupled with UHPLC-(Q) TOF-MS/MS have been widely applied to the screening and identification of active ingredients of TCMs, especially for the screening of TCM monomers for antitumor activity [49,50].

Recent scientific evidence has confirmed the multiple anticancer properties of SO, demonstrating efficacy against breast, gastric, and liver cancer [17,51]. A few monomer compounds, such as ZYG II and 3,3′,4′-trimethylellagic acid (TMEA), have been proven to be responsible for anticancer effects, yet the active ingredients against colon cancer have not been fully clarified, and the mechanism remains unclear [52]. Our research group has been devoted to screening active ingredients from TCMs by CMC coupled with UHPLC-(Q)TOFMS for a long time. In a preceding investigation, a newly discovered bioactive fraction derived from Radix Polygalae was examined, revealing the presence of 17 prominent triterpenoid saponins, notably including onjisaponin B [48]. Furthermore, the major chemical components baicalein and baicalin in *Scutellaria baicalensis* were effectively identified as the active compounds that inhibit the fibrillation of Aβ (1-42) through an assessment of the peak area of individual chemical components in the chromatogram. Following the incubation with an Aβ peptide, further study illustrated that baicalein and baicalin may be anti-Alzheimer's disease agents by inhibiting the formation of Aβ (1–42) fibrils and increasing the viability of PC-12 cells [53]. Based on the successful experience of our previous study, we used CMC firstly screen the potential bioactive compounds from SO-MtOH with anti-proliferative effects in SW620 cells. The constituents within the SO-MtOH that engage in specific interactions with SW620 cells were determined through the use of UHPLC-(Q)TOF-MS/MS. Finally, 4 main components, including ZYG I, ZYG II, ZYG III and OG, were found in the cell lysates with SO-MtOH but not in the blank lysates or final PBS buffer. In addition, it is worth noting that there are still some other potential unidentified compounds with little content in SO-MtOH (e.g., m/z 586.3507, m/z 543.3028, and m/z 934.0136) that also
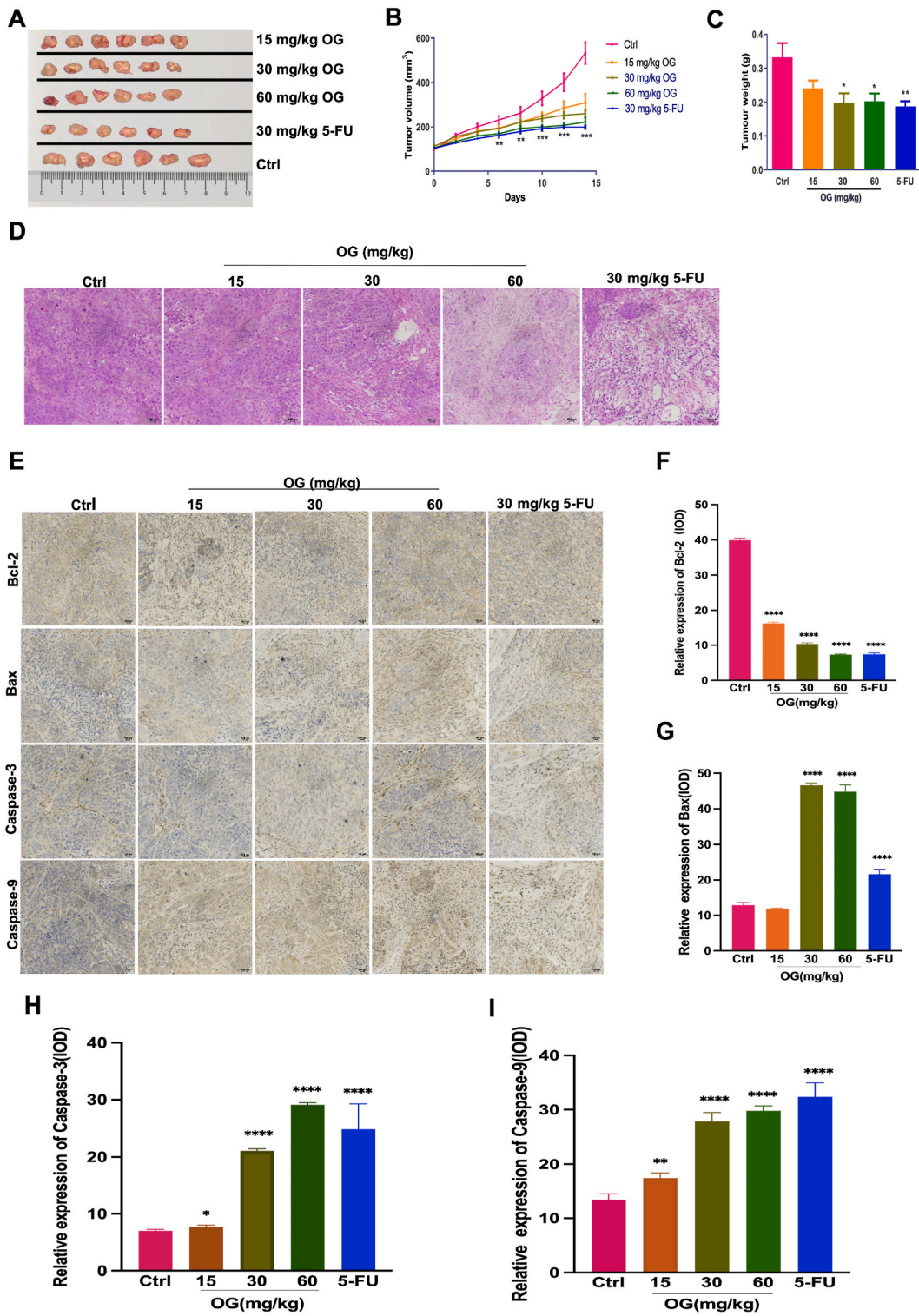
(caption on next page)

Fig. 7. OG inhibist the growth of tumors in a nude mice model carrying SW620 cells. Following successful modelling, the mice were subjected to treatment at varying dosages of 15, 30, and 60 mg/kg/day, as well as with 5-fluorouracil (30 mg/kg/day) administered intraperitoneally. As specified for a duration of 14 days (n = 6, male). (**A**) The stripped tumor of nude mice. (**B**) Summary bar graph of tumor volume. (**C**) Summary bar graph of tumor weight. The application of OG resulted in the inhibition of SW620 cell proliferation in the neoplastic tissue. (**D**) Tumor section images were captured using representative H&E staining methodology, utilizing a microscope at $200 \times$ magnification. The scale bar for these images is 100 μm. (**E**) OG substantially suppresses the upregulation of Bcl-2 and consequently promotes the upregulation of Bax, caspase-3, and caspase-9 in tumor tissue. Fluorescence microscope images of representative IHC tumor sections were obtained at a magnification of $200 \times$, with a scale bar of 100 μm. (**F, G, H, I**) Summary bar graph of Bcl-2, Bax, caspase-3, caspase-9. The data reported in this study represents the mean ± standard deviation (SD) of three independent experiments. The data was analyzed using one-way analysis of variance (ANOVA) with Dunnett's 154 and two-way ANOVA with Tukey's 862 multiple comparisons test. The significance levels for the comparisons are denoted as follows: $*P < 0.05$, $**P < 0.01$, and $***P < 0.001$ vs. control.

interact with SW620 cells. The literature has reported that ZYG II shows excellent anti-colon cancer activity, which further demonstrates that our CMC method is reliable and accurate. In the present study, although this screening preliminarily identified many potential bioactive components with anti-proliferative effects in SW620 cells, we only validated and confirmed the anti-proliferative effect of the major components, including ZYG I, ZYG II, and OG. The results indicated that ZYG II and OG prominently inhibited cell viability in SW620 cells. One of the analyzation conducted suggests that OG prompts the apoptotic process in pancreatic cancer cells, impedes the cell cycle of breast cancer, and induces steatosis in hepatocellular carcinoma cells [54,55]. Nevertheless, the potential anti-colon cancer effect of OG has yet to be documented in existing literature.

The research conducted in this study demonstrated that OG exhibits anti-colon cancer properties by suppressing cell proliferation, migration, and invasion, while also promoting cell apoptosis both *in vitro* and *in vivo*. The mechanistic investigation demonstrated that the efficacy of OG in mitigating colon cancer is associated with its ability to inhibit the PI3K/AKT/mTOR signaling pathway. Furthermore, the blood vessels within tumors are a crucial focus for the management of cancer therapeutics, and the normalization of the tumor vasculature has emerged as a novel therapeutic approach [56]. Our study showed that OG could effectively reduce the viability of HUVECs, suggesting that it may have a potential inhibitory effect on angiogenesis to further improve its anti-colon cancer effect.

5. Conclusions

The present study employed a CMC method for the first time to identify potential bioactive components with anti-colon cancer effects. One of the identified compounds, OG, has been shown to exert inhibitory effects on proliferation, migration, and invasion, as well as to induce apoptosis in colon cancer cells. Mechanistic studies revealed that OG can significantly inhibits the PI3K/AKT/mTOR signaling pathway. In conclusion, our research provides evidence for the identification of anticancer components in TCMs and OG as a new drug against colon cancer.

Institutional review board statement

The animal study protocol received approval from Southwest Medical University (Luzhou, China, License No. 2020362).

Data availability statement

The present study incorporates all relevant figures and data within the confines of this manuscript to substantiate its findings. The dataset supporting the conclusions of this research is accessible from the corresponding author upon justifiable inquiry.

CRediT authorship contribution statement

Chengyang Ni: Writing – original draft. **Liang Yue:** Writing – review & editing. **Mei Ran:** Writing – review & editing, Writing – original draft. **Long Wang:** Visualization. **Feihong Huang:** Conceptualization. **Shuo Yang:** Data curation. **Jia Lai:** Investigation. **Nan Jiang:** Resources. **Xinwu Huang:** Supervision. **Dalian Qin:** Resources. **Hua Li:** Investigation. **Jie Zhou:** Project administration, Formal analysis. **Jing Zeng:** Resources, Methodology. **Anguo Wu:** Writing – review & editing. **Jianming Wu:** Writing – review & editing, Supervision.

Declaration of competing interest

The authors declare that they have no known competing financial interests or personal relationships that could have appeared to influence the work reported in this paper.

Acknowledgements

Appendix A. Supplementary data

Supplementary data to this article can be found online at https://doi.org/10.1016/j.heliyon.2024.e32230.

References

[1] M.I. Gonzaga, L. Grant, C. Curtin, J. Gootee, P. Silberstein, E. Voth, The epidemiology and survivorship of clear cell sarcoma: a national cancer database (ncdb) review, J. Cancer Res. Clin. Oncol. 144 (2018) 1711–1716.

[2] F. Burtin, C.S. Mullins, M. Linnebacher, Mouse models of colorectal cancer: past, present and future perspectives, World J. Gastroenterol. 26 (2020) 1394–1426.

[3] C. Rupnarain, Z. Dlamini, S. Naicker, K. Bhoola, Colon cancer: genomics and apoptotic events, Biol. Chem. 385 (2004) 449–464.

[4] Y. Chen, J. Zou, H. Sun, J. Qin, J. Yang, Metals in traditional Chinese medicinal materials (tcmm): a systematic review, Ecotoxicol. Environ. Saf. 207 (2021) 111311.

[5] P. Zhou, J. Li, Q. Chen, L. Wang, J. Yang, A. Wu, N. Jiang, Y. Liu, J. Chen, W. Zou, J. Zeng, J. Wu, A comprehensive review of genus *sanguisorba*: traditional uses, chemical constituents and medical applications, Front. Pharmacol. 12 (2021) 750165.

[6] N.H. Lee, M.Y. Lee, J.A. Lee, D.J. Dung, C.S. Seo, J.H. Kim, H.K. Shin, Anti-asthmatic effect of *Sanguisorba officinalis* L. And potential role of heme oxygenase-1 in an ovalbumin-induced murine asthma model, Int. J. Mol. Med. 26 (2010) 201–208.

[7] S. Jo, J. Ryu, H. Kim, M. Kim, M.H. Ryu, H. Kim, S.I. Cho, Anti-inflammatory effects of *Sanguisorbae Radix* on contact dermatitis induced by dinitrofluorobenzene in mice, Chin. J. Integr. Med. 26 (2020) 688–693.

[8] S. Park, D.S. Kim, S. Kang, B.K. Shin, Synergistic topical application of salt-processed *Phellodendron Amurense* and *Ssanguisorba officinalis Linne* alleviates atopic dermatitis symptoms by reducing levels of immunoglobulin e and pro-inflammatory cytokines in NC/Nga mice, Mol. Med. Rep. 12 (2015) 7657–7664.

[9] J.H. Yang, J.M. Yoo, W.K. Cho, J.Y. Ma, Ethanol extract of *Sanguisorbae Radix* inhibits mast cell degranulation and suppresses 2,4-dinitrochlorobenzene-induced atopic dermatitis-like skin lesions, Mediat. Inflamm. (2016) 2947390.

[10] W. Zhao, X. Zeng, F. Meng, X. Bi, D. Xu, X. Chen, Q. Li, Y. Han, Structural characterization and in vitro-in vivo evaluation of effect of a polysaccharide from *sanguisorba officinalis* on acute kidney injury, Food Funct. 10 (2019) 7142–7151.

[11] A. Yasueda, H. Kayama, M. Murohashi, J. Nishimura, K. Wakame, K.I. Komatsu, T. Ogino, N. Miyoshi, H. Takahashi, M. Uemura, C. Matsuda, T. Kitagawa, K. Takeda, T. Ito, Y. Doki, H. Eguchi, S. Shimizu, T. Sanguisorba officinalis L. Mizushima, Derived from herbal medicine prevents intestinal inflammation by inducing autophagy in macrophages, Sci. Rep. 10 (2020) 9972.

[12] L. Zhang, S.R. Koyyalamudi, S.C. Jeong, N. Reddy, P.T. Smith, R. Ananthan, T. Longvah, Antioxidant and immunomodulatory activities of polysaccharides from the roots of *sanguisorba officinalis*, Int. J. Biol. Macromol. 51 (2012) 1057–1062.

[13] A. Gawron-Gzella, E. Witkowska-Banaszczak, W. Bylka, M. Dudek-Makuch, A. Odwrot, N. Skrod-zka, Chemical composition, antioxidant and antimicrobial activities of *Sanguisorba officinalis* L. Extracts, Pharm. Chem. J. 50 (2016) 244–249.

[14] M. Szejk-Arendt, K. Czubak-Prowizor, A. Macieja, T. Poplawski, A.K. Olejnik, I. Pawlaczyk-Graja, R. Gancarz, H.M. Zbikowska, Polyphenolic-polysaccharide conjugates from medicinal plants of *Rosaceae/Asteraceae* family protect human lymphocytes but not myeloid leukemia k562 cells against radiation-induced death, Int. J. Biol. Macromol. 156 (2020) 1445–1454.

[15] Z. Wang, W.T. Loo, N. Wang, L.W. Chow, D. Wang, F. Han, X. Zheng, J.P. Chen, Effect of *Sanguisorba officinalis* L. on breast cancer growth and angiogenesis, Expert Opin. Ther. Targets 16 (Suppl 1) (2012) S79–S89.

[16] M.P. Liu, M. Liao, C. Dai, J.F. Chen, C.J. Yang, M. Liu, Z.G. Chen, M.C. Sanguisorba officinalis L. Yao, Synergistically enhanced 5-fluorouracil cytotoxicity in colorectal cancer cells by promoting a reactive oxygen species-mediated, mitochondria-caspase-dependent apoptotic pathway, Sci. Rep. 6 (2016) 34245.

[17] N. Wang, G. Muhetaer, X. Zhang, B. Yang, C. Wang, Y. Zhang, X. Wang, J. Zhang, S. Wang, Y. Zheng, F. Zhang, Z. Wang, *Sanguisorba officinalis* L. Suppresses triple-negative breast cancer metastasis by inhibiting late-phase autophagy via Hif-1alpha/Caveolin-1 signaling, Front. Pharmacol. 11 (2020) 591400.

[18] Y. Matsui, M.F. O'Rourke, S. Hoshide, J. Ishikawa, K. Shimada, K. Kario, Combined effect of angiotensin ii receptor blocker and either a calcium channel blocker or diuretic on day-by-day variability of home blood pressure: the Japan combined treatment with olmesartan and a calcium-channel blocker versus olmesartan and diuretics randomized efficacy study, Hypertension 59 (2012) 1132–1138.

[19] T. Ishimitsu, A. Numabe, T. Masuda, T. Akabane, A. Okamura, J. Minami, H. Matsuoka, Angiotensin-ii receptor antagonist combined with calcium channel blocker or diuretic for essential hypertension, Hypertens. Res. 32 (2009) 962–968.

[20] W. Ma, C. Wang, R. Liu, N. Wang, Y. Lv, B. Dai, L. He, Advances in cell membrane chromatography, J. Chromatogr. A 1639 (2021) 461916.

[21] S. Wang, M. Sun, Y. Zhang, H. Du, L. He, A new a431/cell membrane chromatography and online high performance liquid chromatography/mass spectrometry method for screening epidermal growth factor receptor antagonists from Radix Sophorae Flavescentis, J. Chromatogr. A 1217 (2010) 5246–5252.

[22] M. Sun, W.N. Ma, Y. Guo, Z.G. Hu, L.C. He, Simultaneous screening of four epidermal growth factor receptor antagonists from Curcuma Longa via cell membrane chromatography online coupled with hplc-ms, J. Separ. Sci. 36 (2013) 2096–2103.

[23] L. Feng, Y.H. Xu, S.S. Wang, W. Au-Yeung, Z.G. Zheng, Q. Zhu, P. Xiang, Competitive binding between 4,4'-diphenylmethane-bis(methyl) carbamate and rage ligand mg-h1 on human umbilical vein endothelial cell by cell membrane chromatography, J. Chromatogr., B: Anal. Technol. Biomed. Life Sci. 881–882 (2012) 55–62.

[24] P. Zhou, J.Y. Li, Q. Chen, L. Wang, J. Yang, A.G. Wu, A comprehensive review of genus *Sanguisorba*: traditional uses, chemical constituents and medical applications, Front. Pharmacol. 12 (2021) 750165.

[25] X.P. Gao, J.M. Wu, W.J. Zou, Z.R. Liu, B.G. Li, Screening of the active fractions from *Sanguisorba offcinalis* promoting hematopoiesis. Chin, J. Nat. Med. 2 (2006) 137–140.

[26] C.L. Dang, F.R. Cheng, Influence of radix *Sanguisorbae* on hemorrheology in rabbits, Chinese J Med Phys 3 (1997) 7–8.

[27] S. Zhao, Z.C. Zheng, H. Shen, Effects of radix sanguisorbae, radix angelicae dahuricae and cortex dictamni on the ulcerative colitis in rats, J Clin Med Pract 15 (2011) 1–4.

[28] K.H. Park, D. Koh, K. Kim, Antiallergic activity of a disaccharide isolated from *Sanguisorba offcinalis*, Phytother Res. 18 (2004) 658–662.

[29] K.Y. Wu, X.F. Huang, X.X. Peng, Experimental research on bacteriostasis of borneol, *Polygonum cuspidatum* and *Sanguisorba offcinalis*, Acta Acad Med Jiangxi 36 (1996) 53–55.

[30] H.K. Jia, Efficacy of Coptidis Rhizoma combined with *Sanguisorba Radix* powder for the treatment of acne vulgaris, Guide China Med 10 (2012) 293–294.

[31] K. Tsukahara, S. Moriwaki, T. Fujimura, Y. Takema, Inhibitory effect of an extract of *Sanguisorba offcinalis* L. on ultraviolet-B-induced photodamage of rat skin, Biol. Pharm. Bull. 24 (2001) 998–1003.

[32] X.F. Qin, Y.X. Chen, Research progress in anti-tumor mechanism and drug delivery system of ziyuglycoside, Chinese journal of Pharmaceutics 18 (2020) 180–186.

[33] Y. Hu, T. Xia, J.B. Zhao, Antitumor Effect of *Sanguisorba Offcinalis* Tannins on Liver Cancer Cell SMMC-7721 by MTT and FCM, vol. 5, J Fourth Milit Med Univ., 1998, pp. 550–552.

[34] C.L. Wan, J.H. Chai, X.W. Sun, J.W. Hao, X.F. Sun, The effect and mechanisms of n-butanol extract from *Sanguisorba offcinalis* L. on the proliferation and apoptosis of human liver cancer HepG2 cells, Anti-tumor pharmacy 4 (2014) 112–116.

[35] K.V. Chua, C.S. Fan, C.C. Chen, L.L. Chen, S.C. Hsieh, T.S. Huang, Octyl gallate induces pancreatic ductal adenocarcinoma cell apoptosis and suppresses endothelial-mesenchymal transition-promoted M2-macrophages, HSP90α Secretion, and Tumor Growth, Cells 9 (2019) 91.

[36] K.G. Lima, V.G. Schneider, Rosa, M.C. Garcia, Octyl gallate induces hepatic steatosis in HepG2 cells through the regulation of SREBP-1c and PPAR-gamma gene expression, EXCLI J 19 (2020) 962–971.

[37] M.S. Sales, A. Roy, L. Antony, Octyl gallate and gallic acid isolated from Terminalia bellarica regulates normal cell cycle in human breast cancer cell lines, Biomed. Pharmacother. 103 (2018) 1577–1584.

[38] A.G. Wu, V.K. Wong, W. Zeng, L. Liu, B.Y. Law, Identification of novel autophagic *Radix Polygalae* fraction by cell membrane chromatography and UHPLC-(Q) TOF-MS for degradation of neurodegenerative disease proteins, Sci. Rep. 5 (2015) 17199.

[39] C.C. Liang, A.Y. Park, J.L. Guan, In vitro scratch assay: a convenient and inexpensive method for analysis of cell migration in vitro, Nat. Protoc. 2 (2007) 329–333.

[40] L. Li, F. Wang, J. Zhang, K. Wang, X. De, L. Li, Y. Zhang, Typical phthalic acid esters induce apoptosis by regulating the PI3K/AKT/Bvl-2 signaling pathway in rat insulinoma cells, Ecotoxicol. Environ. Saf. 208 (2021) 111461.

[41] B.C. Giovanella, S.O. Yim, J.S. Stehlin, L.J. Williams Jr., Development of invasive tumors in the "nude" mouse after injection of cultured human melanoma cells, J. Natl. Cancer Inst. 48 (1972) 1531–1533.

[42] X.Y. Lang, Y. Hu, J.P. Bai, J. Wang, X.Y. Qin, R. Lan, Coeloglossum Viride Var. Bracteatum extract attenuates MPTP-induced neurotoxicity in vivo by restoring BNDF-TRKB and FGF2-AKT signaling axis and inhibiting rip1-driven inflammation, Front. Pharmacol. 13 (2012) 903235, 2.

[43] C. Wu, M. Yao, W. Li, B. Cui, H. Dong, Y. Ren, C. Yang, C. Gan, Simultaneous determination and pharmacokinetics study of six triterpenes in rat plasma by UHPLC-MS/MS after oral administration of *sanguisorba officinalis* L. Extract, Molecules 23 (2018).

[44] S. Kim, S. Oh, H.B. Noh, S. Ji, S.H. Lee, J.M. Koo, C.W. Choi, H.P. Jhun, In vitro antioxidant and anti-propionibacterium acnes activities of cold water, hot water, and methanol extracts, and their respective ethyl acetate fractions, from *Sanguisorba officinalis* L. Roots, Molecules 23 (2018).

[45] J.M. Kim, S.H. Choi, G.H. Shin, J.H. Lee, S.R. Kang, K.Y. Lee, H.S. Lim, T.S. Kang, O.H. Lee, Method validation and measurement uncertainty for the simultaneous determination of synthetic phenolic antioxidants in edible oils commonly consumed in Korea, Food Chem. 213 (2016) 19–25.

[46] K. Lkhagvasuren, J.K. Kim, Ziyuglycoside ii induces caspases-dependent and caspases-independent apoptosis in human colon cancer cells, Toxicol. Vitro 59 (2019) 255–262.

[47] B.T. Hennessy, D.L. Smith, P.T. Ram, Y. Lu, G.B. Mills, Exploiting the pi3k/akt pathway for cancer drug discovery, Nat. Rev. Drug Discov. 4 (2005) 988–1004.

[48] M.E. Wall, Camptothecin and taxol: discovery to clinic, Med. Res. Rev. 18 (1998) 299–314.

[49] T. Dong, C. Li, X. Wang, L. Dian, X. Zhang, L. Li, S. Chen, R. Cao, L. Li, N. Huang, S. He, X. Lei, Ainsliadimer a selectively inhibits ikkalpha/beta by covalently binding a conserved cysteine, Nat. Commun. 6 (2015) 6522.

[50] W. Hou, Z. Luo, G. Zhang, D. Cao, D. Li, H. Ruan, B.H. Ruan, L. Su, H. Xu, Click chemistry-based synthesis and anticancer activity evaluation of novel c-14 1,2,3-triazole dehydroabietic acid hybrids, Eur. J. Med. Chem. 138 (2017) 1042–1052.

[51] Y. Zhong, X.-Y. Li, F. Zhou, Y.-J. Cai, R. Sun, R.-P. Liu, Ziyuglycoside ii inhibits the growth of digestive system cancer cells through multiple mechanisms, Chin. J. Nat. Med. 19 (2021) 351–363.

[52] C. Bai, Y. Sun, X. Pan, J. Yang, X. Li, A. Wu, D. Qin, S. Cao, W. Zou, J. Wu, Antitumor effects of trimethylellagic acid isolated from *Sanguisorba officinalis* L. On colorectal cancer via angiogenesis inhibition and apoptosis induction, Front. Pharmacol. 10 (2019) 1646.

[53] L. Yu, A.G. Wu, V.K. Wong, L.Q. Qu, N. Zhang, D.L. Qin, W. Zeng, B. Tang, H.M. Wang, Q. Wang, B.Y. Law, The new application of UHPLC-DAD-TOF/MS in identification of inhibitors on beta-amyloid fibrillation from *Scutellaria Baicalensis*, Front. Pharmacol. 10 (2019) 194.

[54] M.S. Sales, A. Roy, L. Antony, S.K. Banu, S. Jeyaraman, R. Manikkam, Octyl gallate and gallic acid isolated from *Terminalia bellarica* regulates normal cell cycle in human breast cancer cell lines, Biomed. Pharmacother. 103 (2018) 1577–1584.

[55] K.V. Chua, C.S. Fan, C.C. Chen, L.L. Chen, S.C. Hsieh, T.S. Huang, Octyl gallate induces pancreatic ductal adenocarcinoma cell apoptosis and suppresses endothelial-mesenchymal transition-promoted m2-macrophages, hsp90alpha secretion, and tumor growth, Cells 9 (2019).

[56] H. Li, Z. Wang, Z. Chen, T. Ci, G. Chen, D. Wen, R. Li, J. Wang, H. Meng, R. Bryan Bell, Z. Gu, G. Dotti, Z. Gu, Disrupting tumour vasculature and recruitment of a PDL1- loaded platelets control tumour metastasis, Nat. Commun. 12 (2021) 2773.